Electrical Manipulation of Quantum Coherence in a Two-Level Molecular System

Likun Wang[1], Dan Bai[1], Yunpeng Xia[1], and W. Ho[1,2,*]

[1]*Department of Physics and Astronomy, University of California, Irvine, Irvine, California 92697-4575, USA*
[2]*Department of Chemistry, University of California, Irvine, Irvine, California 92697-2025, USA*

We report the manipulation of ultrafast quantum coherence of a two-level single hydrogen molecular system by employing static electric field from the sample bias in a femtosecond terahertz scanning tunneling microscope. A H_2 molecule adsorbed on the polar Cu_2N surface develops an electric dipole and exhibits a giant Stark effect. An avoided crossing of the quantum state energy levels is derived from the resonant frequency of the single H_2 two levels in a double-well potential. The dephasing time of the initial wave packet can also be changed by applying the electric field. The electrical manipulation for different tunneling gaps in three dimensions allows quantification of the surface electrostatic fields at the atomic scale. Our work demonstrated the potential application of molecules as controllable two-level molecular systems.

Quantum coherence at the ultrafast timescale is invaluable to quantum information processing [1–4]. The femtosecond to picosecond coherent oscillations of superposition states in a two-level system (TLS) enable ultrafast operations to store and process information that outperforms the most powerful classical systems. It is thus paramount to be able to locally manipulate the resonant frequency and decoherence time of the ultrafast quantum coherence of an individual TLS [1,3,5]. The facile method of electrical manipulation of ultrafast coherence at the atomic scale with known environment of the TLS has yet to be demonstrated.

Scanning tunneling microscope (STM) combined with time-domain techniques [6–22] provides an effective platform to study the quantum coherence with unprecedented spatial resolution. With a magnetic atom functionalized tip, pulsed electron spin resonance has been performed on single atoms and molecules to measure and manipulate the spin coherence at the nanosecond timescale [11,15]. The free coherent evolution of a coupled spin-1/2 system was also demonstrated by direct current (dc) pump-probe spectroscopy in the STM [16]. On the other hand, laser combined STM [6,7,12] has been employed to probe the ultrafast electron [17,18], spin [8], or polaron [20] dynamics with nanoscale spatial resolution. The successful detection of ultrafast quantum coherence in single molecules proclaimed the remarkable accomplishments by terahertz (THz) [9,21,23] and optical STM [10,13,19,22].

In this Letter, we demonstrate the electrical manipulation of the ultrafast quantum coherence in a single H_2 molecule trapped inside the STM junction. Our femtosecond THz-STM enabled us to monitor variations of the coherent oscillations while changing the applied sample bias to impose the dc electric field on the molecule. The oscillation frequency varied along an asymmetric parabola as a function of the sample bias. The dephasing time T_2^* was greatly extended by increasing the total electric field experienced by the H_2. An avoided crossing between the ground and excited state energy levels of H_2 can be determined from the close agreement between the experimental results and the fittings. By operating the STM tip in three-dimensional space, we systematically investigated the influence of the tip-substrate separation and the underlying surface atomic composition on our electrical manipulation method. This is a major step forward from previous efforts, in which the coherence measurement over a TLS was demonstrated [21]. In this work, a complete manipulation of the quantum coherence is realized by changing the dc electric field.

Our femtosecond THz-STM scheme employed pairs of delayed femtosecond THz pulses focused into the STM junction (see Supplemental Material [24] for additional details). The H_2 molecules were adsorbed on the monolayer Cu_2N islands grown on the Cu(001) surface. A charge transfer took place between the polar Cu_2N surface [31] and H_2 molecule, giving rise to a nonzero charge displacement, as deduced from the electric dipole moment difference in the H_2 [32–34]. The total electric field $\mathbf{F}_{tot}$ experienced by the H_2 molecule was a combination of the underlying surface electrostatic field $\mathbf{F}_{surface}$ and the dc field $\mathbf{F}_{dc}$ from the externally applied sample bias [35]. By exclusively tuning the sample bias, the magnitude and direction of $\mathbf{F}_{tot}$ could be controlled precisely with a fixed $\mathbf{F}_{surface}$. Three situations are shown in Figs. 1(a)–1(c) where $\mathbf{F}_{tot}$ was set to be negative, zero, and positive, respectively.

A H_2 molecule trapped in the STM junction can be described as a TLS in a double-well potential [21,36], similar to the well-known TLS of gaseous ammonia molecule. The tunnel coupling between the original basis
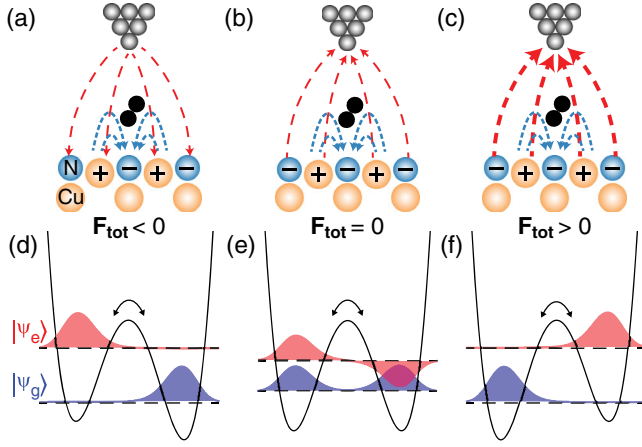
FIG. 1. Electrical manipulation of the quantum states showing the schematics of the total electric field experienced by the H₂ molecule in the STM junction. (a) The total electric field points toward the Cu₂N surface ($F_{tot} < 0$), (b) becomes zero ($F_{tot} = 0$), and (c) points toward the tip ($F_{tot} > 0$). The blue and red dashed arrows represent the electrostatic field from the Cu₂N surface and dc field from the applied sample bias, respectively. The thicker arrows in (c) represent stronger dc field due to the higher sample bias. (d)–(f) Schematics of the ground and excited eigenstate wave function distribution of the TLS in the double well potential corresponding to (a)–(c). Blue and red shaded curves represent the ground and excited state wave functions, respectively.

states leads to two eigenstates delocalized in the double-well potential, as shown schematically in Figs. 1(d)–1(f). In accordance with the setting of $\mathbf{F}_{tot}$ in Figs. 1(a)–1(c), the asymmetry of the double-well potential and the two eigenstate energy levels can be tuned [Figs. 1(d)–1(f)]

[37]. The tunnel-coupled ground and excited state wave functions are also redistributed. The highly localized wave functions in Fig. 1(d) become delocalized and distributed equally in the two wells when the $\mathbf{F}_{tot}$ is zero and the double well potential becomes symmetric in Fig. 1(e).

The energy separation of the H₂ TLS falls in the THz range, thus making it possible to prepare a superposition of the eigenstates by THz photon absorption and monitor its ultrafast coherent evolution through pump-probe measurements in our femtosecond THz-STM [21]. The THz light behaves simultaneously as photon (particle) and field (wave) in our measurement of the rectification current [21,38]. The rectification current is due entirely to the ac voltage oscillations developed across the nonlinear H₂ molecular junction by the THz field, which is altered with the absorption of the THz photon by the H₂ molecular system. As a result, the rectification current is a convoluted signal from both particle and wave nature of the THz pulses. The ultrafast coherence varied with the sample bias while maintaining the same tip-substrate separation and tip position marked in Fig. 2(a). In Fig. 2(b), the oscillation period gradually changed with sample bias, showing the largest period near 45 mV. In the corresponding fast Fourier transform (FFT) spectra to extract the oscillation frequency, an asymmetric parabola with the minimum at 0.28 THz was revealed at 45 mV in Fig. 2(c).

For a TLS in the double-well potential, the observed energy separation 2Ω has contributions from the energy splitting 2Δ of the two basis states under Stark effect and the tunnel coupling A between them [Fig. 2(d)]. By applying the second-order Stark effect on the basis states and including A, we obtain the Hamiltonian of the system:

$$\mathbf{H} = \begin{pmatrix} E_0 - \left(\boldsymbol{\mu}_a \cdot \mathbf{F}_{tot} + \frac{1}{2}\boldsymbol{\alpha}_a \cdot \mathbf{F}_{tot}^2 \right) & -A \\ -A & E_0 - \left(\boldsymbol{\mu}_b \cdot \mathbf{F}_{tot} + \frac{1}{2}\boldsymbol{\alpha}_b \cdot \mathbf{F}_{tot}^2 \right) \end{pmatrix}.$$

The energy separation between the two eigenstates of this Hamiltonian is given by

$$\Delta E = 2\Omega = \sqrt{\left(\Delta\boldsymbol{\mu} \cdot \mathbf{F}_{tot} + \frac{1}{2}\Delta\boldsymbol{\alpha} \cdot \mathbf{F}_{tot}^2 \right)^2 + 4A^2},$$

where $\mathbf{F}_{tot} = \mathbf{F}_{surface} + \mathbf{F}_{dc}$, $\Delta\boldsymbol{\mu} = \boldsymbol{\mu}_b - \boldsymbol{\mu}_a$, and $\Delta\boldsymbol{\alpha} = \boldsymbol{\alpha}_b - \boldsymbol{\alpha}_a$ are the total electric field, the dipole moment, and polarizability differences between the two basis states, respectively.

A comparison in Fig. 2(e) shows the energy level shift calculated from the model Hamiltonian for the basis states and eigenstates as a function of the sample bias. Under the Stark effect, the energy levels of the basis states cross. An avoided level crossing emerges by incorporating the tunnel coupling in calculating the eigenstates. The ground and excited eigenstates are linear combinations of the basis states, $|g\rangle = \cos(\theta/2)|a\rangle + \sin(\theta/2)|b\rangle$ and $|e\rangle = -\sin(\theta/2)|a\rangle + \cos(\theta/2)|b\rangle$, with the mixing angle θ defined by the ratio of the tunnel coupling to half of the energy splitting of the two basis states, $\tan\theta = (A/\Delta)$. At a negative sample bias far away from the avoided crossing region, θ approaches a minimum value of zero and the eigenstate $|g\rangle(|e\rangle)$ is mostly composed of the basis state $|a\rangle(|b\rangle)$. The maximum value of $\pi/2$ for θ is obtained at the tuning point in the avoided crossing region where the eigenfunctions are delocalized equally in the two potential
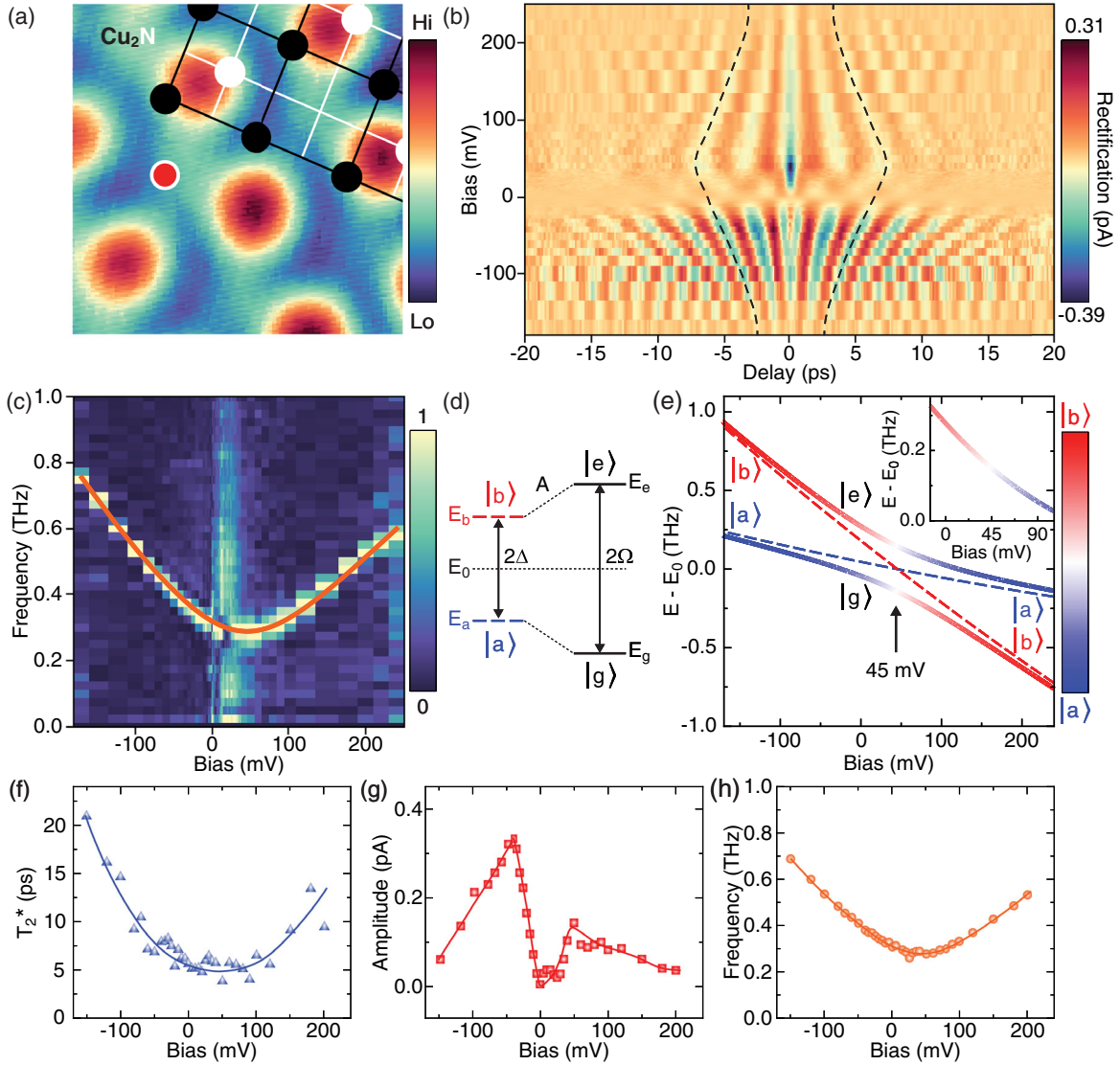
FIG. 2. Electrical manipulation of quantum states from the ultrafast coherence measurement. (a) Constant-current topography of Cu_2N; image size 13.0 Å × 13.0 Å. Scanning condition: −20 mV/0.1 nA. The Cu_2N lattice structure is superimposed on the topography with lines connecting the Cu (black) and N (white) atoms in the two sublattices. (b) Color map of a series of THz pump-probe measurements as a function of sample bias. The sample bias is varied after turning the feedback off at −30 mV/40 pA. The dashed lines serve as a guide to show the change of oscillation period. (c) Color map of FFT results from the pump-probe measurements in (b). The superimposed orange curve is the fitting of the data. For clarity, the intensity of all spectra is normalized positively to the color palette with range (0,1). (d) Energy level diagram of the basis states ($|a\rangle$, $|b\rangle$) and eigenstates ($|g\rangle$, $|e\rangle$) of the TLS in a double well potential. (e) Propagation of the avoided level crossing under the influence of the sample bias. Colors represent the calculated mixing angle θ. (f)–(h) The bias dependent dephasing time T_2^*, coherent oscillation amplitude, and oscillation frequency extracted from the fitting of the oscillations in the time-domain results in (b). The blue and red lines in (f) and (g) are guides to the eye. The orange line in (h) is the same fitted curve as in (c).

wells [Fig. 1(e)]. As illustrated by the color palette in Fig. 2(e), the majority component of the eigenstate $|g\rangle$($|e\rangle$) undergoes a transition from the basis state $|a\rangle$($|b\rangle$) on the left side of the avoided crossing region to the basis state $|b\rangle$($|a\rangle$) on the right side, as manipulated by the sample bias. The energy separation ΔE of the TLS can be employed to closely fit the observed resonant frequency, as shown in Fig. 2(c).

We also performed numerical fitting to the time domain results in Fig. 2(b) to extract the coherent properties of the H_2 TLS under the external $\mathbf{F}_{dc}$ [Figs. 2(f)–2(h)]. Interferences among multiple closely related excited states in the H_2 TLS lead to a fast dephasing of the initial wave packet (see Supplemental Material [24]), which is closely related to the decoherence time [21]. This dephasing time T_2^* reaches a minimum of around 5 ps at the tuning point of
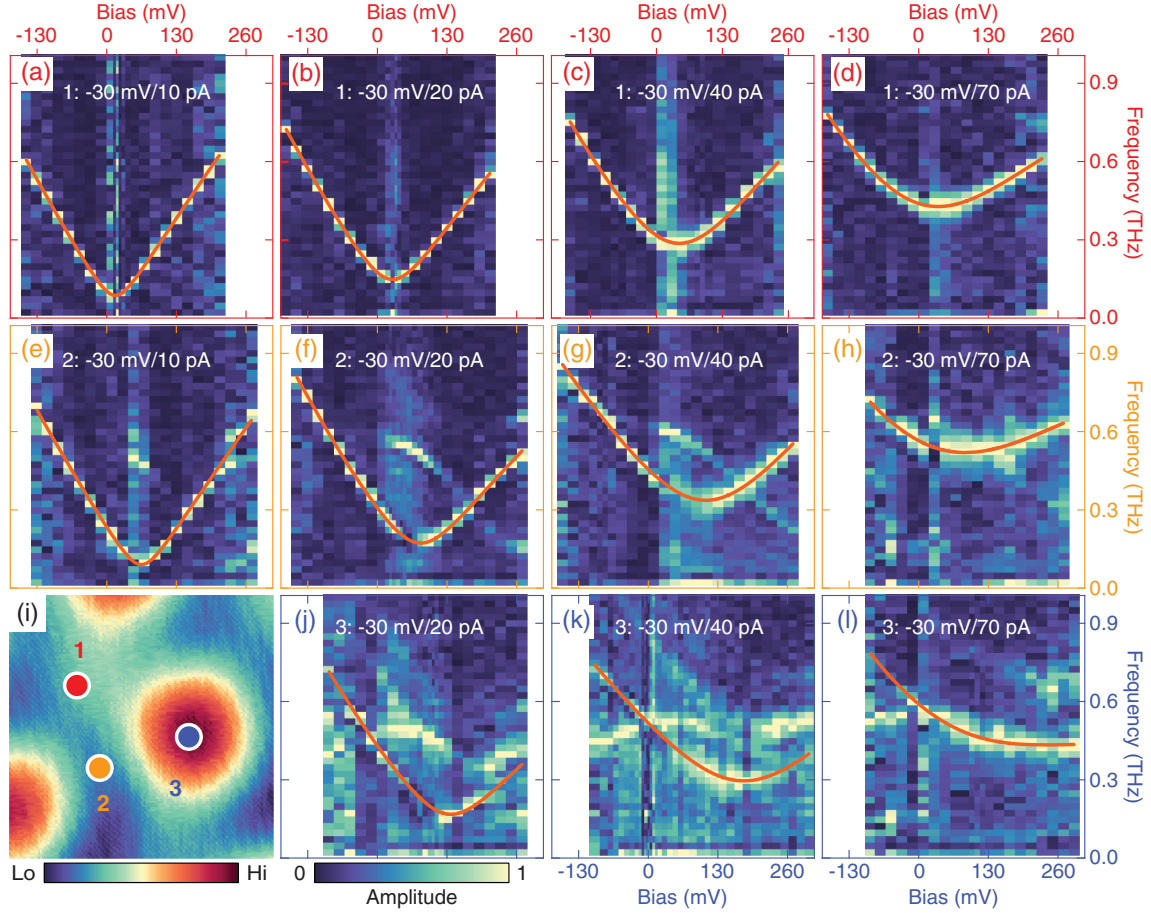
FIG. 3. Panorama of the quantum state manipulation. (a)–(d), (e)–(h), and (j)–(l) Color maps of the sample bias-controlled oscillation frequency with various tip-substrate separations over positions 1, 2, and 3 marked in (i). The tip-substrate separation is controlled by ramping the tunneling current to the value labeled in each panel before turning off the feedback. Orange curves are the fittings of the data. For clarity, the intensity of all the spectra is normalized positively to the color palette with range (0,1). (i) Constant current topography of the Cu_2N surface; image size 7.4 Å by 7.4 Å. Scanning condition: -20 mV/0.1 nA.

45 mV where $\mathbf{F}_{tot}$ is 0 [Fig. 2(f)]. Upon increasing the magnitude of $\mathbf{F}_{tot}$, T_2^* is extended, reaching a maximum of 20 ps at -150 mV. Additional discussions of the T_2^*, coherent oscillation amplitude and frequency can be found in Supplemental Material [24].

The tunnel coupling strongly depends on the tip-substrate separation. As shown in Figs. 3(a)–3(d) and Supplemental Material [24], an obvious blueshift is observed on the overall shape of the parabola as the tip approaches the surface. For each parabola, the minimum resonant frequency at the tuning point represents the tunnel coupling energy in THz unit. As the tip-substrate separation is decreased, the central barrier of the double-well potential can be lowered, thus increasing the tunnel coupling and the corresponding resonant frequency. The parabola shape also shows an increased asymmetry for decreasing tip-substrate separation, which indicates a change of the dipole moment and the polarizability of the H_2 molecule. In addition, the corresponding sample bias of the minimum resonant frequency shows a slight increase from Figs. 3(a) to 3(d),

which can be explained by a larger $\mathbf{F}_{surface}$ experienced by the H_2 molecule as it is likely pushed closer to the surface.

The Cu_2N surface is fully covered by H_2 under our experimental conditions. There is always a single H_2 trapped in the junction when the tip moves to different locations of the surface. Figures 3(e)–3(h) and Figs. 3(j)–3(l) show variations of the parabola at positions 2 and 3 as labeled in Fig. 3(i). The sample bias differs for the minimum resonant frequency at each position. When the tip is placed over these three different positions with the same set point, the applied $\mathbf{F}_{dc}$ does not exhibit consequential differences. However, the underlying $\mathbf{F}_{surface}$ varies due to the different elemental composition of the Cu_2N lattice. As a result, the $\mathbf{F}_{tot}$ experienced by the H_2 changes and is reflected in the different parabolas shown for the three positions.

By fitting each parabola in Fig. 3 to the eigenstate energy separation $\Delta E = 2\Omega$, we can quantify the parameters in the Hamiltonian. An analysis of the tip-substrate separation (see Supplemental Material [24]) was performed to convert
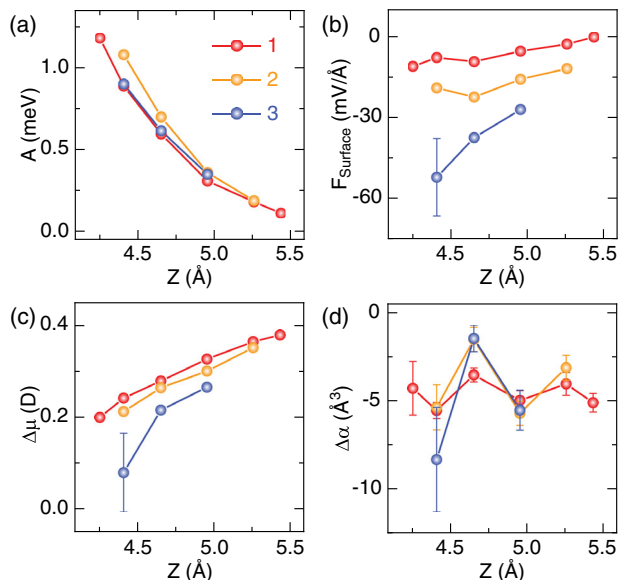
FIG. 4. Quantitative description of the H_2 two-level system (TLS). (a)–(d) Fitting parameters of the tunnel coupling, surface electrostatic field, dipole moment difference, and polarizability difference of the TLS, respectively. All parameters are extracted from the corresponding fitting curves in Fig. 3 and Supplemental Material [24].

the sample bias to electric field. As shown in Fig. 4(a), the tunnel coupling A increases exponentially as the tip approaches the surface, in accordance with the lowering of the central barrier in the double-well potential. No obvious difference in the tunnel coupling is observed over these three different positions indicated in Fig. 3(i), which is consistent with negligible variations of the tip-substrate separation in the constant current mode. The $\mathbf{F}_{surface}$ experienced by the H_2 shows a linear increase upon decreasing the tip-substrate separation [Fig. 4(b)]. Unlike the tunnel coupling, $\mathbf{F}_{surface}$ varies significantly over these three positions, consistent with the different elemental composition of the underlying Cu_2N lattice. The dipole moment and polarizability differences for the two basis states can also be extracted from the fitting [Figs. 4(c) and 4(d)]. In addition to the fitted parabola, other parabolas in Fig. 3 could be modeled by coupling of the H_2 in the STM junction to neighboring H_2 molecules nearest the junction.

In summary, we have established an electrical method to locally manipulate the ultrafast quantum coherence in a single molecular TLS with atomic-scale spatial resolution. Both the coherent oscillation frequency and dephasing time T_2^* can be precisely manipulated by varying the sample bias. The combination of shorter oscillation period and longer T_2^* allows a larger number of ultrafast quantum operations within the decoherence time. This paradigm of electrical manipulation should be readily applicable to other molecular TLS [39,40]. This work points to the possibility of quantum information processing based on

molecules with the advantages of having widely tunable properties through chemical synthesis.

*To whom all correspondence should be addressed.
 wilsonho@uci.edu

[1] S. M. Clark, Kai-Mei C. Fu, T. D. Ladd, and Y. Yamamoto, Quantum Computers Based on Electron Spins Controlled by Ultrafast Off-Resonant Single Optical Pulses, Phys. Rev. Lett. 99, 040501 (2007).

[2] J. Berezovsky, M. H. Mikkelsen, N. G. Stoltz, L. A. Coldren, and D. D. Awschalom, Picosecond coherent optical manipulation of a single electron spin in a quantum dot, Science 320, 349 (2008).

[3] D. Press, K. De Greve, P. L. McMahon, T. D. Ladd, B. Friess, C. Schneider, M. Kamp, S. Höfling, A. Forchel, and Y. Yamamoto, Ultrafast optical spin echo in a single quantum dot, Nat. Photonics 4, 367 (2010).

[4] R. Hildner, D. Brinks, and N. F. van Hulst, Femtosecond coherence and quantum control of single molecules at room temperature, Nat. Phys. 7, 172 (2011).

[5] D. Press, T. D. Ladd, B. Zhang, and Y. Yamamoto, Complete quantum control of a single quantum dot spin using ultrafast optical pulses, Nature (London) 456, 218 (2008).

[6] Y. Terada, S. Yoshida, O. Takeuchi, and H. Shigekawa, Real-space imaging of transient carrier dynamics by nanoscale pump-probe microscopy, Nat. Photonics 4, 869 (2010).

[7] T. L. Cocker, V. Jelic, M. Gupta, S. J. Molesky, J. A. J. Burgess, G. D. L. Reyes, L. V. Titova, Y. Y. Tsui, M. R. Freeman, and F. A. Hegmann, An ultrafast terahertz scanning tunnelling microscope, Nat. Photonics 7, 620 (2013).

[8] S. Yoshida, Y. Aizawa, Z. Wang, R. Oshima, Y. Mera, E. Matsuyama, H. Oigawa, O. Takeuchi, and H. Shigekawa, Probing ultrafast spin dynamics with optical pump-probe scanning tunnelling microscopy, Nat. Nanotechnol. 9, 588 (2014).

[9] T. L. Cocker, D. Peller, P. Yu, J. Repp, and R. Huber, Tracking the ultrafast motion of a single molecule by femtosecond orbital imaging, Nature (London) 539, 263 (2016).

[10] S. Li, S. Chen, J. Li, R. Wu, and W. Ho, Joint Space-Time Coherent Vibration Driven Conformational Transitions in a Single Molecule, Phys. Rev. Lett. 119, 176002 (2017).

[11] K. Yang, W. Paul, S.-H. Phark, P. Willke, Y. Bae, T. Choi, T. Esat, A. Ardavan, A. J. Heinrich, and C. P. Lutz, Coherent spin manipulation of individual atoms on a surface, Science 366, 509 (2019).

[12] S. Yoshida, H. Hirori, T. Tachizaki, K. Yoshioka, Y. Arashida, Z.-H. Wang, Y. Sanari, O. Takeuchi, Y. Kanemitsu, and H. Shigekawa, Subcycle transient scanning tunneling spectroscopy with visualization of enhanced terahertz near field, ACS Photonics 6, 1356 (2019).

[13] M. Garg and K. Kern, Attosecond coherent manipulation of electrons in tunneling microscopy, Science **367**, 411 (2020).

[14] M. Müller, N. Martín Sabanés, T. Kampfrath, and M. Wolf, Phase-resolved detection of ultrabroadband THz pulses inside a scanning tunneling microscope junction, ACS Photonics **7**, 2046 (2020).

[15] P. Willke, T. Bilgeri, X. Zhang, Y. Wang, C. Wolf, H. Aubin, A. Heinrich, and T. Choi, Coherent spin control of single molecules on a surface, ACS Nano **15**, 17959 (2021).

[16] L. M. Veldman, L. Farinacci, R. Rejali, R. Broekhoven, J. Gobeil, D. Coffey, M. Ternes, and A. F. Otte, Free coherent evolution of a coupled atomic spin system initialized by electron scattering, Science **372**, 964 (2021).

[17] S. Yoshida, Y. Arashida, H. Hirori, T. Tachizaki, A. Taninaka, H. Ueno, O. Takeuchi, and H. Shigekawa, Terahertz scanning tunneling microscopy for visualizing ultrafast electron motion in nanoscale potential variations, ACS Photonics **8**, 315 (2021).

[18] M. Abdo, S. Sheng, S. Rolf-Pissarczyk, L. Arnhold, J. A. J. Burgess, M. Isobe, L. Malavolti, and S. Loth, Variable repetition rate THz source for ultrafast scanning tunneling microscopy, ACS Photonics **8**, 702 (2021).

[19] M. Garg, A. Martin-Jimenez, Y. Luo, and K. Kern, Ultrafast photon-induced tunneling microscopy, ACS Nano **15**, 18071 (2021).

[20] C. Guo et al., Probing Nonequilibrium Dynamics of Photo-excited Polarons on a Metal-Oxide Surface with Atomic Precision, Phys. Rev. Lett. **124**, 206801 (2020).

[21] L. Wang, Y. Xia, and W. Ho, Atomic-scale quantum sensing based on the ultrafast coherence of an H_2 molecule in an STM cavity, Science **376**, 401 (2022).

[22] M. Garg, A. Martin-Jimenez, M. Pisarra, Y. Luo, F. Martín, and K. Kern, Real-space subfemtosecond imaging of quantum electronic coherences in molecules, Nat. Photonics **16**, 196 (2022).

[23] D. Peller, L. Z. Kastner, T. Buchner, C. Roelcke, F. Albrecht, N. Moll, R. Huber, and J. Repp, Sub-cycle atomic-scale forces coherently control a single-molecule switch, Nature (London) **585**, 58 (2020).

[24] See Supplemental Material at http://link.aps.org/supplemental/10.1103/PhysRevLett.130.096201 for details of experiment methods, supplemental text, and figures, which includes Refs. [25–30].

[25] F. D. Natterer, F. Patthey, and H. Brune, Distinction of Nuclear Spin States with the Scanning Tunneling Microscope, Phys. Rev. Lett. **111**, 175303 (2013).

[26] S. Li, A. Yu, F. Toledo, Z. Han, H. Wang, H. Y. He, R. Wu, and W. Ho, Rotational and Vibrational Excitations of a Hydrogen Molecule Trapped within a Nanocavity of Tunable Dimension, Phys. Rev. Lett. **111**, 146102 (2013).

[27] F. D. Natterer, F. Patthey, and H. Brune, Resonant-enhanced spectroscopy of molecular rotations with a scanning tunneling microscope, ACS Nano **8**, 7099 (2014).

[28] R. Temirov, S. Soubatch, O. Neucheva, A. C. Lassise, and F. S. Tautz, A novel method achieving ultra-high geometrical resolution in scanning tunnelling microscopy, New J. Phys. **10**, 053012 (2008).

[29] C. Weiss, C. Wagner, C. Kleimann, M. Rohlfing, F. S. Tautz, and R. Temirov, Imaging Pauli Repulsion in Scanning Tunneling Microscopy, Phys. Rev. Lett. **105**, 086103 (2010). 5

[30] T. Choi, C. D. Ruggiero, and J. A. Gupta, Incommensurability and atomic structure of $c(2 \times 2)$N/Cu(100): A scanning tunneling microscopy study, Phys. Rev. B **78**, 035430 (2008).

[31] M. Schneiderbauer, M. Emmrich, A. J. Weymouth, and F. J. Giessibl, CO Tip Functionalization Inverts Atomic Force Microscopy Contrast via Short-Range Electrostatic Forces, Phys. Rev. Lett. **112**, 166102 (2014).

[32] S. Li, D. Yuan, A. Yu, G. Czap, R. Wu, and W. Ho, Rotational Spectromicroscopy: Imaging the Orbital Interaction between Molecular Hydrogen and an Adsorbed Molecule, Phys. Rev. Lett. **114**, 206101 (2015).

[33] H. Wang, S. Li, H. He, A. Yu, F. Toledo, Z. Han, W. Ho, and R. Wu, Trapping and Characterization of a single hydrogen molecule in a continuously tunable nanocavity, J. Phys. Chem. Lett. **6**, 3453 (2015).

[34] S. Li, G. Czap, J. Li, Y. Zhang, A. Yu, D. Yuan, H. Kimura, R. Wu, and W. Ho, Confinement-induced catalytic dissociation of hydrogen molecules in a scanning tunneling microscope, J. Am. Chem. Soc. **144**, 9618 (2022).

[35] S. A. Empedocles and M. G. Bawendi, Quantum-confined Stark effect in single CdSe nanocrystallite quantum dots, Science **278**, 2114 (1997).

[36] J. A. Gupta, C. P. Lutz, A. J. Heinrich, and D. M. Eigler, Strongly coverage-dependent excitations of adsorbed molecular hydrogen, Phys. Rev. B **71**, 115416 (2005).

[37] C. Lotze, M. Corso, K. J. Franke, F. von Oppen, and J. I. Pascual, Driving a macroscopic oscillator with the stochastic motion of a hydrogen molecule, Science **338**, 779 (2012).

[38] J. Yao, P. J. Wagner, Y. Xia, G. Czap, and W. Ho, Atomic-scale rectification and inelastic electron tunneling spectromicroscopy, Nano Lett. **22**, 7848 (2022).

[39] B. Verlhac, N. Bachellier, L. Garnier, M. Ormaza, P. Abufager, R. Robles, M.-L. Bocquet, M. Ternes, N. Lorente, and L. Limot, Atomic-scale spin sensing with a single molecule at the apex of a scanning tunneling microscope, Science **366**, 623 (2019).

[40] G. Czap, P. J. Wagner, F. Xue, L. Gu, J. Li, J. Yao, R. Wu, and W. Ho, Probing and imaging spin interactions with a magnetic single-molecule sensor, Science **364**, 670 (2019).